

Theory of excitation bands of hydrogen in bcc metals and of their observation by neutron scattering

R. C. Casella

National Measurement Laboratory, National Bureau of Standards, Washington, D.C. 20234

(Received 7 October 1982)

I consider the possibility that the excited-state oscillator wave functions of dilute hydrogen in bcc metals overlap sufficiently with nearest-neighbor occupancy sites so as to produce hydrogenic energy bands, analogous to electronic energy bands in narrow-band semiconductors. The theory is motivated by the experiments of Magerl *et al.* as well as the earlier observation of ground-state tunnel splitting by Wipf *et al.*, demonstrating quantum coherence in the motion of the hydrogen, despite the necessity of correlated motion by the surrounding metal atoms. Because of the latter complication, the relevant overlap integrals are not calculated from first principles. The band structures are given for the first (nondegenerate) and second (doubly degenerate) excitations ω_I and ω_{II} of the local oscillators, *modulo* a few irreducible overlap integrals, which are then determined by comparison with experiment. The fact that the experimental bandwidths for inelastic neutron scattering from dilute hydrogen in V, Nb, and Ta satisfy $\Gamma(V) > \Gamma(Nb) > \Gamma(Ta)$ at room temperature (Rush, Magerl, and Rowe) finds a natural explanation in the theory. It is shown that the ω_I and ω_{II} bandwidths satisfy $\Delta E_{II}/\Delta E_I = (H_{II}/H_I)\Upsilon$, where H_I and H_{II} are irreducible overlap integrals and Υ is an (almost) universal constant for H in bcc metals, determined (essentially) by the geometry of the tetrahedrally coordinated hydrogen occupancy sites. On the basis of the band structure that I obtain, I estimate that $\Upsilon \simeq \frac{3}{4}$. Based upon physical reasoning, the relation $(H_{II}/H_I) = (\omega_{II}/\omega_I)^2$ is proposed. Given the (model-consistent) empirical result, $\omega_{II}/\omega_I \simeq 2^{1/2}$, this leads to the prediction $\Delta E_{II}/\Delta E_I \simeq \frac{3}{2}$, to be compared with the neutron-measured ratios $\Gamma_{II}/\Gamma_I = 1.3$ and 2.0 for dilute hydrogen trapped at O and N impurities in Nb metal at $T = 4$ and 10 K, respectively. The variation in Γ_{II}/Γ_I is attributed to perturbations of the intrinsic hydrogen bands by the trapping impurities, which are necessary for low-temperature observation, if one is to prevent coagulation of the hydrogen atoms into the ϵ phase of NbH. The differential cross section for inelastic neutron scattering from hydrogen in band states is related theoretically to that for H in local oscillator states. With appropriate rescaling, the band structure that I obtain for hydrogen can also be applied to the case of trapped positive muons in bcc metals.

I. INTRODUCTION

The investigation via neutron scattering of hydrogen in bcc metals, both nominally pure and doped with interstitial or substitutional impurities, is currently an area of active experimental research.¹⁻⁴ Of particular interest is the recent observation of tunnel splitting of the local-oscillator ground state of hydrogen in the presence of dilute oxygen impurities in niobium.² (The splitting is presumably enhanced by a lowering of the potential barrier between two tetrahedral hydrogen occupancy sites as a consequence of the strain field produced by the nearby oxygen interstitial.) This experimental observation of tunnel splitting clearly demonstrates that

at sufficiently low temperatures the motion of hydrogen in these metals exhibits *quantum coherence*, despite possible self-trapping effects associated with the correlated motions of the surrounding metal atoms. Following the success of the two-well model in explaining the neutron-induced ground-state tunneling transitions,² the theory of neutron-induced transitions to coherent superpositions of *excited oscillator* states in the assumed two-well trap has been investigated by this author.^{5,6} Here, I examine transitions to the excited states from a different vantage, based upon the hypothesis that, even in undoped systems, motion of the hydrogen, when in excited oscillator levels, exhibits sufficient coherence that quasi-Bloch states form a natural basis for calcula-

tion, leading to itinerant hydrogenic energy bands, analogous to the electronic energy bands in narrow-band semiconductors. From this point of view, when a hydrogen trapped near an impurity is excited, say, by inelastic neutron scattering, to a state O (100 meV) above the ground state, the final state is not simply an excitation of the local two-well system, as was assumed in Ref. 5. Rather, it lies in an excitation band, that of dilute itinerant hydrogen in an excited state in the pure metal, modified however by the strain field of the nearby impurity. This hypothesis is suggested by two experimental facts. (a) Semiquantitatively, the neutron-measured excitation bands for hydrogen associated with interstitial O (or N) impurities in Nb and those for hydrogen in the α phase of undoped Nb are nearly the same,⁷ although detailed quantitative differences exist.^{3,4} (b) The excitation bands of either are wider than is the case for the ordered (β or ϵ phase) hydride NbH,^{3,4} where the excitations are more likely optical-mode phonon bands, associated with the oscillations of the hydrogens about fixed positions, while participating in cooperative lattice vibrations of the hydride system.

Thus motivated, I have calculated the energy-band structure for dilute hydrogen in otherwise pure bcc metals, in the tight-binding approximation, using basis states which are linear combinations of the local-oscillator hydrogen states at each interstitial occupancy site. (Apart from scale, the resulting band structure also applies to that of positive muons in bcc metals, as obtained experimentally via the weak decays of captured accelerator-produced pions.) In V, Nb, and Ta the occupancy sites are assumed to lie at the vertices of the Wigner-Seitz (WS) cell, as shown in Fig. 1. As illustrated there, each possible occupancy site (vertex), such as A , is tetrahedrally coordinated with four near-neighbor metal atoms (a, b, c, d) which form a cage, leading to a local oscillator potential at each vertex. Moreover, each occupancy site (A) is also tetrahedrally coordinated with four nearest-neighbor occupancy sites (1, 2', 3', and 4). It is the overlap between the near-neighbor excited-oscillator wave functions which, when acting on the crystal potential produced by the interaction between the hydrogen and the lattice of metal atoms, leads to the band structure I obtain, much as the overlap between electronic wave functions centered at various sites in a narrow-band semiconductor leads to the electronic band structure within the customary tight-binding [linear combination of atomic orbitals (LCAO)] approximation. In addition to the obvious mass difference between that of the electron and that of the proton (or captured μ^+), together with its electronic shielding cloud, there are other significant distinctions to be drawn between the two analogs. (i) In the electronic case,

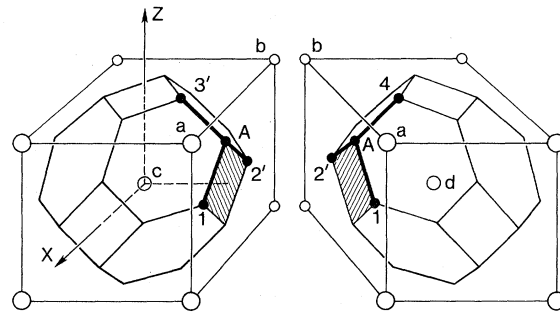


FIG. 1. Cutaway view of the hydrogen occupancy-site configuration in bcc metals. All vertices of the Wigner-Seitz cell are energetically equivalent. The hydrogen at site A experiences short-range forces from the metal atoms in the tetrahedral array a, b, c, d , about it. The nearest-neighbor occupancy sites 1, 2', 3', and 4 are also tetrahedrally coordinated about A .

the potential active in the overlap term is a linear combination of the *same* local atomic potentials which give rise, in the absence of overlap, to the atomic energy levels (in single-particle approximation). Here, the local oscillator potential giving rise to the oscillator wave functions is valid only in the neighborhood of each vertex of the WS cell, being, in fact, an effective potential resulting from expanding the sum of nearby metallic cage potentials. Whereas this expansion may be quite appropriate near the vertices (see below), in the regions of maximum overlap between near-neighbor oscillator wave functions, the harmonic potential is not valid and one must revert to the actual shield-proton— (or μ^+) metal-atom interaction potential. (ii) The presence of the proton (or muon) plus its electronic shielding cloud at a given site (such as A in Fig. 1) displaces the nearby metal atoms, at a, b, c , and d (shown undisplaced) as well as other more distant atoms. Therefore, as is well known, when tunneling to a nearest-neighbor position, not only the hydrogen (or muon), but also its associated metal-atom displacement field must undergo the transition. Thus a first-principles calculation of the relevant overlap terms can become quite involved and, in any event, must depend upon the details of the assumed hydrogen—metal-atom interaction potential. Not surprisingly, as a consequence of symmetry, it turns out that of the many overlap terms which arise in the band-structure calculation, most can be expressed in terms of a few *irreducible* overlap integrals, differing from these few by known phase factors. In the phenomenological model considered here, these few irreducible overlap integrals can be

treated as parameters to be fitted by experiment, rather than to be obtained by *a priori* calculation. (iii) The distortion effects discussed above can lead to self-trapping, effectively destroying the coherence between wave functions centered at energetically equivalent sites. Here, I rely on the success of the two-well model in describing the transitions between the tunnel-split components of the oscillator *ground* state, where, as noted earlier, coherence is clearly in evidence experimentally.^{1,2} If, when in the excited oscillator state, phase coherence is maintained over distances of order, a few times the lattice parameter a , then quasibands will result. Moreover, the symmetry of these bands within the Brillouin zone will be that of the effective rigid-band model employed here. Also, even when short lived, these band states can play an important role as effective final states, when describing the scattering of neutrons from hydrogen in bcc metals.

In view of comment (i) above, one may question the use of the oscillator states as a basis. Their use is suggested by experiment. If one assumes that the potential due to interaction of a hydrogen atom (shielded proton) near site A in Fig. 1 with the metal atoms a , b , c , and d can be obtained by summing central potentials $V(|\vec{x}-\vec{R}_i|)$, describing its interaction with each, and expanding in terms of small displacements of the hydrogen from A , then, subject to the condition $r|d^2V/dr^2| \gg |dV/dr|$ at $r=(\frac{5}{16})^{1/2}a$, it follows that the first (nondegenerate) and second (doubly degenerate) local-oscillator excitation frequencies, ω_I and ω_{II} , satisfy the relation $\omega_{II}=2^{1/2}\omega_I$. This relation is obeyed experimentally to within 10% for all systems reported in Ref. 3. Thus, apart from widths, the local-oscillator model for the motion of the hydrogen (and its distortion field) gives a quite good phenomenological description of the data. This fact is sometimes cited as evidence for the complete localization of the hydrogen, but the latter need not follow. In the narrow-band approximation, states consisting of linear combinations of these local-oscillator states [cf. Eqs. (6) and (7), Sec. II] can equally well describe itinerant hydrogen in bands centered about these energies, whence the desired (experimental) ratio between the excitation peaks is maintained. Apart from widths, the cross section $d^2\sigma/d\Omega d\epsilon$ for inelastic neutron scattering from hydrogen in narrow-band states made up of oscillator states centered on a Bravais lattice is nearly the same as is obtained for scattering from hydrogen localized in single oscillator states. As is demonstrated in Sec. II, the two cross sections differ by the replacement of an energy δ function in the expression for the latter by a finite density-of-states function $g(E)$ which appears in that for the case of energy bands. The cross sections

become identical in the limit of vanishing bandwidth. When there is more than one hydrogen occupancy site per unit cell, the expression for $d^2\sigma/d\Omega d\epsilon$ is generally more complex, but, in leading approximation, reduces to the same form as that obtained for the case of the Bravais lattice.

Thus the itinerant band model has several attractive features. However, there exists a possible difficulty. As discussed earlier, within the effective rigid-band model the matrix elements in the relevant secular determinants can all be expressed in terms of a few irreducible overlap integrals of the type

$$H_{nn'} = \int d^3x f_n^*(\vec{x}-\vec{\rho}) H f_{n'}(\vec{x}-\vec{\rho}'), \quad (1)$$

where the interaction Hamiltonian H satisfies

$$H = -(1/2m_1)\nabla^2 + \sum_{L,i} V(\vec{x}-\vec{L}-\vec{r}_i). \quad (2)$$

Here, f_n and $f_{n'}$ are local-oscillator wave functions, $\vec{\rho}$ and $\vec{\rho}'$ lie on nearby vertices of the WS cell (cf., Fig. 1), and the sum in Eq. (2) runs over all metal atom sites \vec{r}_i in the unit cell and over all cells \vec{L} . Also, $\hbar=1$ throughout. First, consider diagonal terms of the type given by Eq. (1) with $n'=n$ and $\vec{\rho}'=\vec{\rho}$. For this case, a second-order expansion about $\vec{x}=\vec{\rho}$ of the potential in Eq. (2) leads to the approximate oscillator Hamiltonian

$$H = \text{const} - (1/2m_1)\nabla^2 + \frac{1}{2}m_1\omega_I^2(\vec{x}-\vec{\rho})_{||}^2 + \frac{1}{2}m_1\omega_{II}^2(\vec{x}-\vec{\rho})_{\perp}^2 + \dots, \quad (3)$$

valid near $\vec{x}=\vec{\rho}$. Ignoring the constant and higher order terms in Eq. (3), substitution in Eq. (1) yields the local-oscillator energy $(n_I + \frac{1}{2})\omega_I + (n_{II1} + n_{II2} + 1)\omega_{II}$, times a normalization integral, equal to unity. When $\vec{\rho}' \neq \vec{\rho}$, one can attempt to estimate the magnitude of the integral (1) by writing it in the form

$$H_{nn'} = \epsilon \int d^3x f_n^*(\vec{x}-\vec{\rho}) f_{n'}(\vec{x}-\vec{\rho}'), \quad (4)$$

where ϵ is a scalar parameter, having the dimensions of energy. The dimensionless integral in Eq. (4) can be readily evaluated and typically turns out to be quite small. For example, when $n'=n=(n_I, n_{II1}, n_{II2})=(1,0,0)$, which corresponds to the first excitation equal to ω_I , and $\vec{\rho}'-\vec{\rho}$ is chosen to connect nearest neighbors, I find, using the experimental result³ $\omega_I=106 \pm 1$ meV for $\text{NbN}_{0.004}\text{H}_{0.003}$ and setting m_1 equal to the proton mass,

$$H_I = 5 \times 10^{-4} \epsilon. \quad (5)$$

As will be seen in Sec. III, detailed calculation of the band structure centered at ω_I , treating the overlap integral H_I as an undetermined parameter, leads to a bandwidth, $\Delta E_I=8H_I$. (This result holds in

nearest-neighbor approximation, but is not altered appreciably when small second-nearest-neighbor corrections are introduced.) Now, if one selects the scale ϵ in Eq. (5) equal to the oscillator excitation energy ω_I , then one obtains for the estimated band width, $\Delta E_I = 0.4$ meV, a result considerably smaller than the experimental width Γ_I [full width at half maximum (FWHM)] = 11 meV at $T = 10$ K.³ This discrepancy is the source of possible difficulty. However, as noted earlier in (i), in the region of maximum overlap between the near-neighbor wave functions, the local-oscillator potential in Eq. (3) is no longer valid. Far from the potential minima, the strength of the (typically exponential) hydrogen-metal-atom interaction can greatly exceed the scale set by ω_I . Indeed, the hydrogen-metal-atom repulsive interaction can be so great in the regions of maximum overlap between the unperturbed local-oscillator wave functions that, in higher order approximation, the wave functions are rather small there, and the dominant contribution to the band widths comes instead from the residual overlap in the saddle-point regions midway between the vertices of the WS cell. In either case, the scale ϵ in Eq. (5) can, in principle, be very much larger than the excitation energies of the local oscillators, allowing consonance with the experimental widths. As stated earlier in (ii), no attempt will be made to compute the renormalized overlap terms from first principles. Instead, as will become clear in Sec. III, apart from overall scale, the general features of the energy-band structure can be made evident without *a priori* knowledge of their values. This is particularly so for the first excited band, centered at ω_I , but also holds, to lesser extent, for the second band, centered at ω_{II} , although detailed results for the latter depend upon an assumption concerning the ratio of the two irreducible overlap integrals which enter in nearest-neighbor approximation. Also, for both bands, including next-nearest-neighbor overlap integrals introduces a few additional parameters, leading to further perturbations on the pristine band structure.

I turn now to a derivation of the differential cross section for inelastic neutron scattering from dilute hydrogen in narrow energy bands in metals (Sec. II). Section III contains further details of the excited-state hydrogen (or μ^+) band-structure calculation and the results thereof. Comparison is made with experiment in Sec. IV. Conclusions are stated in Sec. V.

II. DIFFERENTIAL CROSS SECTION FOR INELASTIC NEUTRON SCATTERING

I first show that for sufficiently narrow itinerant hydrogen bands in metals, when the possible hydro-

gen occupancy sites form a Bravais lattice, the differential cross section for neutron-induced interband transitions reduces to that which results from neutron-induced transitions among local-oscillator states. Then the modified result is derived for the case of interband transitions when the excited bands have finite width. Finally, the case of more than one hydrogen occupancy site per unit cell is treated. For simplicity the proofs are given in detail only for the case of one occupancy site per primitive cell, and for a low-temperature limit, in which the initial hydrogenic state is a Bloch sum of local oscillators, each in its ground state. Thus the initial (*I*) and final (*F*) hydrogenic states are given by the relations

$$\psi_I^{\vec{k}}(\vec{x}) = N^{-1/2} \sum_L e^{i\vec{k}\cdot\vec{L}} f_0(\vec{x} - \vec{L}) \quad (6)$$

and

$$\psi_F^{\vec{k}'}(\vec{x}) = N^{-1/2} \sum_{L'} e^{i\vec{k}'\cdot\vec{L}'} f_{ex}(\vec{x} - \vec{L}'), \quad (7)$$

where f_0 and f_{ex} are the ground and excited local-oscillator hydrogen wave functions, respectively. \vec{k} and \vec{k}' are the initial and final hydrogen wave vectors and N is the number of unit cells. From the standard Fermi pseudopotential

$$V_F(\vec{x}) = (2\pi a/m)\delta(\vec{x}), \quad (8)$$

with the use of a normalization for the reduced *T*-matrix t_{FI} such that the Heisenberg *S* matrix reads

$$S_{FI} = \delta_{FI} + 2\pi t_{FI} \delta(E_F - E_I), \quad (9)$$

it follows that

$$t_{FI} = (2\pi a/m) \int d^3x e^{-i\vec{q}\cdot\vec{x}} \psi_F^{\vec{k}'}(\vec{x}) \psi_I^{\vec{k}}(\vec{x}). \quad (10)$$

$\vec{q} = \vec{k}_F - \vec{k}_I$ is the momentum transfer to the neutron, m is its mass, and a is the suitably weighted low-energy *np* scattering length. Keeping only the leading terms with $\vec{L}' = \vec{L}$ in Eq. (10) (narrow-band approximation), it follows that

$$t_{FI} = (2\pi a/m) \delta(\vec{k}' - \vec{k} + \vec{q}, \vec{K}) \tilde{F}(\vec{q}). \quad (11)$$

Here \vec{K} is a principal vector of the reciprocal lattice and, following the notation of Ref. 5, $\tilde{F}(\vec{q})$ is the transition form factor for the local oscillator:

$$\tilde{F}(\vec{q}) = \int d^3x e^{-i\vec{q}\cdot\vec{x}} f_{ex}^*(\vec{x}) f_0(\vec{x}). \quad (12)$$

Summing over the final momenta \vec{k}_F and \vec{k}' of the neutron and hydrogen, the total cross section σ implied by Eq. (11) is given by the relation

$$\sigma = (1/k_I m) |\bar{a}|^2 \int d^3 k_F |\tilde{F}(\vec{q})|^2 \delta(k_F^2/2m - k_I^2/2m + E_{\text{ex}}(\vec{k} + \vec{K} - \vec{q}) - E_0(\vec{k})) . \quad (13)$$

For hydrogen bands so narrow that one can neglect the wave-vector dependence of the band energies E_{ex} and E_0 , differentiation of Eq. (13) with respect to solid angle Ω yields the differential cross section

$$\frac{d\sigma}{d\Omega} = (k_F/k_I) |\bar{a}|^2 |\tilde{F}(\vec{q})|^2 , \quad (14)$$

precisely the result one would get for a single isolated local oscillator.⁵ (The lattice Debye-Waller factor is, by definition, included in \bar{a} .⁵)

In the above treatment, the theoretical absorption peak is sharp, and experimental widths must be attributed to other effects. When the excited band $E_{\text{ex}}(\vec{k})$ has finite width, the double differential neutron cross section $d^2\sigma/d\Omega d\epsilon$ can have a finite width, even in the absence of other effects. When the oscillator *ground-state* band remains flat, as is assumed here, the average over the initial hydrogen wave vectors, coupled with the finite width of $E_{\text{ex}}(\vec{k})$ produces a width to the neutron band, even at zero temperature. If this source of the absorption band width becomes dominant, then $d^2\sigma/d\Omega d\epsilon$ is given by an expression of the form given by Eq. (14), multiplied by a density-of-states function $g(E)$ associated with the dispersion of the excited hydrogen energy band, as will now be demonstrated.

Letting ω be the energy transfer to the neutron, i.e.,

$$\omega = \epsilon - \epsilon_I = k_F^2/2m - k_I^2/2m , \quad (15)$$

and differentiating Eq. (13) with respect to Ω and ϵ , it follows that

$$\left(\frac{d^2\sigma}{d\Omega d\epsilon} \right)_I = (k_F/k_I) |\bar{a}|^2 |\tilde{F}(\vec{q})|^2 \times \delta(\omega + E_{\text{ex}}(\vec{k} + \vec{K} - \vec{q}) - E_0(\vec{k})) . \quad (16)$$

Generally, $|I\rangle = |\alpha, \vec{k}\rangle$ denotes the initial proton state, and α is the band index in $E_\alpha(\vec{k})$. Taking a thermal average

$$\frac{d^2\sigma}{d\Omega d\epsilon} = (1/Z) \sum_I e^{-\beta E_I} (d^2\sigma/d\Omega d\epsilon)_I , \quad (17)$$

where Z is the partition sum,

$$Z = \sum_I e^{-\beta E_I} = \sum_{\alpha, \vec{k}} e^{-\beta E_\alpha(\vec{k})} , \quad (18)$$

and $\beta = 1/k_B T$. For temperatures T sufficiently low

that only the lowest band is occupied, only those terms with $\alpha=0$ contribute to Z . In the limit where the width of the ground-state band (but not that of the excited band) is ignored, we may set $E_0(\vec{k})=0$ without loss of generality, whence $Z=N$, the number of unit cells in the crystal. Equations (16) and (17) then lead to the result

$$\frac{d^2\sigma}{d\Omega d\epsilon} = (k_F/k_I) |\bar{a}|^2 |\tilde{F}(\vec{q})|^2 g , \quad (19)$$

where

$$g = (1/N) \sum_k \delta(\omega + E_{\text{ex}}(\vec{k} + \vec{K} - \vec{q})) = (1/N) \sum_k \delta(\omega + E_{\text{ex}}(\vec{k})) . \quad (20)$$

Letting $E(\vec{k}) = E_{\text{ex}}(\vec{k}) - \Delta$ where Δ is the band gap,

$$g = (1/N) \sum_k \delta(-|\omega| + E(\vec{k}) + \Delta) . \quad (21)$$

Finally, let $E = |\omega| - \Delta$ be the neutron energy *loss* relative to Δ , the threshold energy for inducing transitions to the excited band. From Eq. (21),

$$g(E) = (1/N) \sum_k \delta(E(\vec{k}) - E) . \quad (22)$$

It is clear that $g(E)$ represents the excited-band density-of-states function (normalized to unity). In the absence of other broadening mechanisms $g(E)$ determines the shape of the absorption band for the inelastic scattering of a neutron from a single proton which is initially in the oscillator ground state.

For the special case, considered earlier in this section, when the *excited* band is also flat, $E(\vec{k})=0$ for all \vec{k} and Eq. (22) assumes the form

$$g(E) = \delta(E) = \delta(|\omega| - \Delta) . \quad (23)$$

Equation (19) then describes the excitation by a neutron of a single proton in an isolated local-oscillator state, and Δ assumes the value of the first excitation energy of the oscillator. Whether or not the excited band has finite width, since Eq. (22) implies that $\int dE g(E) = 1$, integration of Eq. (19) over energies encompassing the excitation band leads to an expression for $d\sigma/d\Omega$ which is identical to that given by Eq. (14). This completes the proof of the assertions for the case when the hydrogen occupancy sites form a Bravais lattice and the degeneracy of the excited oscillator state is ignored.

I next consider briefly the general case when each unit cell contains more than one equilibrium hydro-

gen occupancy site and account is taken of the degeneracy of the excited oscillator states. Let h be the number of sites per unit cell and d be the degeneracy of the oscillator states from which the band states are constructed. (For tetrahedral sites in a bcc metal, $h=6$. Also, $d=1$ for the oscillator ground

state and first excitation ω_I , whereas $d=2$ for the second excitation ω_{II} . Cf. Sec. III.) If one substitutes the general band states $\psi_{\alpha}^{\vec{k}}$ and $\psi_{\alpha'}^{\vec{k}'}$ obtained, in principle, from solution of the band problem into Eq. (10), then it can be shown that

$$\frac{d^2\sigma}{d\Omega d\epsilon} = (k_F/k_I) |\bar{a}|^2 (1/Nh) \sum_{\vec{k}} \sum_{\alpha} \sum_{\alpha'} |F_{\alpha'\alpha}(\vec{q}, \vec{k})|^2 \delta(\omega + E_{\alpha'}(\vec{k} - \vec{q}) - E_{\alpha}(\vec{k})). \quad (24)$$

Here

$$F_{\alpha'\alpha}(\vec{q}, \vec{k}) = \sum_{a=1}^h \sum_{n'=1}^d e^{-i\vec{q} \cdot \vec{\rho}_a} \langle E_{\alpha'}(\vec{k} - \vec{q}) | a, n' \rangle \langle a, 0 | E_{\alpha}(\vec{k}) \rangle F_{n'0}^a(\vec{q}), \quad (25)$$

where $\vec{\rho}_a$ gives the hydrogen site positions within the cell and $F_{n'0}^a(\vec{q})$ is the transition form factor of the anisotropic local oscillator at $\vec{\rho}_a$:

$$F_{n'0}^a(\vec{q}) = \int d^3x e^{-i\vec{q} \cdot \vec{x}} f_{n'a}^*(\vec{x}) f_{0a}(\vec{x}). \quad (26)$$

Coefficients such as $\langle a, n | E_{\alpha}(\vec{k}) \rangle$ describe the eigenvector solutions of the band equations. For our present purpose, we need only note that, in narrow-band approximation, they satisfy the normalization-completeness relation

$$\sum_{a=1}^h \sum_{n=1}^d |\langle a, n | E_{\alpha}(\vec{k}) \rangle|^2 = 1. \quad (27)$$

To proceed, I shall approximate Eq. (25) by replacing these coefficients by their rms value $(1/hd)^{1/2}$ times a \vec{k} -dependent phase factor of modulus one. Assuming, once again, that the ground-state band is flat and averaging over the phases,

$$\frac{d^2\sigma}{d\Omega d\epsilon} = (k_F/k_I) |\bar{a}|^2 |\hat{F}(\vec{q})|^2 g(\omega), \quad (28)$$

where

$$|\hat{F}(\vec{q})|^2 = (1/h) \sum_{a=1}^h \sum_{n'=1}^d |F_{n'0}^a(\vec{q})|^2 \quad (29)$$

and

$$g(\omega) = (1/hd) \sum_{\alpha=1}^{hd} (1/N) \sum_{\vec{k}} \delta(\omega + E_{\alpha}(\vec{k})). \quad (30)$$

$g(\omega)$ is the multicomponent excited-state band density-of-states function, normalized to unity. (Also, the oscillator ground-state energy has again been chosen as the reference level.) As before, in the limit of vanishing width for the excited oscillator band, Eq. (30) reduces to the simpler form

$$g(\omega) = \delta(|\omega| - \Delta). \quad (31)$$

Since it follows from either Eq. (30) or Eq. (31) that $\int d\omega g(\omega) = 1$, integration of Eq. (28) over the excitation band leads to the result

$$\frac{d\sigma}{d\Omega} = (k_F/k_I) |\bar{a}|^2 |\hat{F}(\vec{q})|^2. \quad (32)$$

Equation (32) is of the same form as Eq. (14).

III. STRUCTURE OF THE ITINERENT HYDROGEN BANDS

To ascertain the nature of the excited hydrogen bands in bcc metals, a realistic calculation must take into account the existence of the six crystallographically inequivalent interstitial hydrogen-occupancy sites within the primitive cell (see Fig. 2). Thus when dealing with Bloch states consisting of linear combinations of the local-oscillator wave functions in the first (nondegenerate) state of excitation ω_I , a

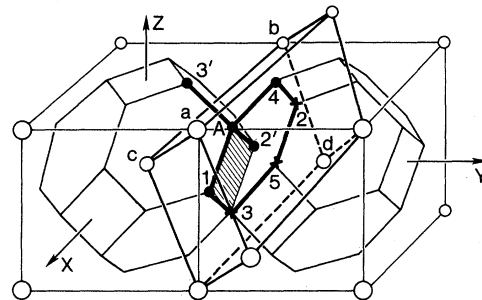


FIG. 2. Primitive cell. Six crystallographically inequivalent sites $A, 1, \dots, 5$ occur on a hexagon within the cell. As drawn, the nearest-neighbor (relative to A) sites $2'$ and $3'$ lie outside the cell. These are crystallographically equivalent to sites 2 and 3 , and the site 5 is equivalent to a second-nearest neighbor of A (cf. Fig. 1.)

6×6 Hamiltonian matrix results for each value of wave vector \vec{k} . The bands associated with the doubly degenerate local-oscillator excitation ω_{II} are derived from a secular determinant obtained from a 12×12 Hamiltonian matrix. For the ω_I bands, in nearest-neighbor approximation, each nonvanishing matrix element can be expressed as a known phase factor $\exp(\phi_{ij})$ times a single irreducible overlap integral H_I . In this approximation, all nonvanishing matrix elements giving rise to the ω_{II} bands are similarly expressible in terms of either of two possible irreducible overlap integrals. Since the excited-oscillator wave functions associated with both the ω_I and ω_{II} excitations have the same symmetry as p -orbital cubic harmonics, they are conveniently represented by arrows in a graphical representation of the various overlap integrals, as shown in Fig. 3. To complete the correspondence between each graph and its associated overlap integral, the appropriate diagram is to be considered as embedded in a representation of the three-dimensional crystal by superposing it on a cube face, such as that with shaded inner square in Fig. 1 or Fig. 2. Then, the wave functions, symbolized by the arrows in the graph, may be thought of as multiplying, left and right, the Hamiltonian [given by Eq. (2)] containing potential terms centered on the bcc host-metal lattice, thus forming the integrand of the so-specified overlap integral. So interpreted, Fig. 3(a) represents the single irreducible overlap integral H_I which, in nearest-neighbor approximation, determines the ω_I bands. Figure 3(d) represents the sole irreducible second-nearest-neighbor overlap integral in the 6×6 Hamiltonian matrix for the ω_I band. The quantity H_I may be thought of as a common scale factor in that matrix, whence, in units of H_I , the structure of the

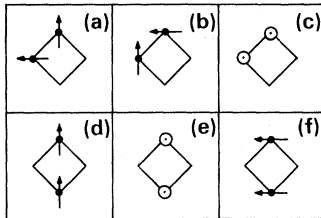


FIG. 3. Diagrams for the various irreducible overlap integrals. Arrows signify the symmetry of the p -orbital cubic harmonics which characterize the excited oscillator states from which the Bloch states are constructed. Graphs (a)–(c) designate nearest-neighbor overlap integrals, (d)–(f) second-nearest-neighbor terms. Graphs (a) and (d) refer to the first (ω_I) excitation band; (b), (c), (e), and (f) belong to the second (ω_{II}) band.

ω_I bands is uniquely determined in nearest-neighbor approximation. Including second-nearest-neighbor corrections, the structure of the ω_I bands is specified by the parameter

$$Y = I_{(d)}/I_{(a)}, \tag{33}$$

where the values of the relevant overlap integrals I are symbolized by their associated graphs [subscripts (a)–(f)]. Thus the detailed shape of the bands depends upon the value of Y , but for small values of $|Y|$, does not differ appreciably from the case $Y=0$, corresponding to the nearest-neighbor approximation. Results I obtain for the ω_I bands are given in Fig. 4, where the solid and dashed curves correspond to $Y=0$ and $Y=-0.2$, respectively. The crude estimate of the ω_I bandwidth employed in Sec. I, namely $\Delta E_I = 8H_I$, follows by inspection of Fig. 4.

In nearest-neighbor approximation, diagrams for the two irreducible overlap integrals which appear in the 12×12 Hamiltonian matrix determining the ω_{II} bands are shown in Figs. 3(b) and 3(c) of Fig. 3. Letting H_{II} ($=I_{(b)}$) be the common scale factor (unit of energy) for these bands, their structure is specified by the parameter

$$S = I_{(c)}/I_{(b)}. \tag{34}$$

That is, unlike the ω_I bands, the shape of the ω_{II}

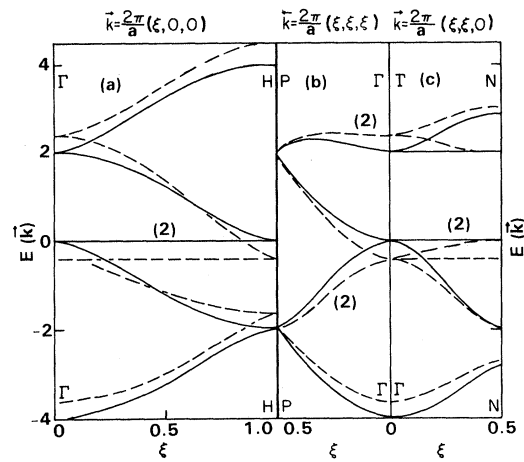


FIG. 4. Band structure $E(\vec{k})$ for the ω_I bands. $E(\vec{k})$ is given for $\vec{k} = (2\pi/a)(\xi, \eta, \zeta)$ along (a) [100], (b) [111], and (c) [110]. Solid curves: nearest-neighbor approximation ($Y=0$). Dashed curves: Next-nearest neighbors included ($Y=-0.2$). (See text.) The energy scale is equal to the overlap integral H_I . The zero of energy is equal to that of the isolated local oscillator, excited by an amount ω_I .

bands is not unique in nearest-neighbor approximation. It appears reasonable to assume $S < 1$. The energy-band structure I obtain for $S=0.5$ in nearest-neighbor approximation is shown in Fig. 5 for various slices in the Brillouin zone. It is perhaps worth noting that setting $S=0$ results in dispersionless bands, with additional accidental degeneracies, not dictated by symmetry. For example, under this artificial assumption, not only are the bands flat, but also sixfold-degenerate bands occur, whereas the maximum dimension of the irreducible representations of the relevant group of the wave vector is 3 at $\vec{k}=0$ and is less than or equal to 2 elsewhere in the zone interior. Even for finite S , two artifacts of the nearest-neighbor approximation may be found in the ω_{II} band structure (see Fig. 5). (i) At a given value of \vec{k} , for each solution E , there exists another at $-E$. (The zero of energy in Fig. 5 has been selected equal to the energy of the isolated local oscillator, excited by ω_{II} .) (ii) Letting $\vec{k}=(2\pi/a)(\xi, \eta, \zeta)$, there

exist band crossings and some zero slopes at $\xi=\frac{1}{2}$, which corresponds to a pseudo-zone-boundary, that of a cubic zone of $\frac{1}{2}$ the volume of the dodecahedral zone and inscribed therein. Such a zone would result if the unit cell in real space were the full cube of volume a^3 rather than the smaller primitive cell of volume $a^3/2$ for the bcc lattice (cf. Fig. 2). These artifacts are removed when the second-nearest-neighbor integrals [Figs. 3(e) and 3(f)] are included in the 12×12 matrix. This situation for the ω_{II} bands is to be contrasted with that for the ω_I bands where, apart from minor shifts of these bands, only the accidental degeneracy of the flat band in the [110] direction is removed by including Fig. 3(d), i.e., for nonzero Y . (See Fig. 4.) Defining the following ratios of irreducible overlap integrals (cf. Fig. 3):

$$\begin{aligned} T &= I_{(e)}/I_{(b)}, \\ U &= I_{(f)}/I_{(b)}, \end{aligned} \quad (35)$$

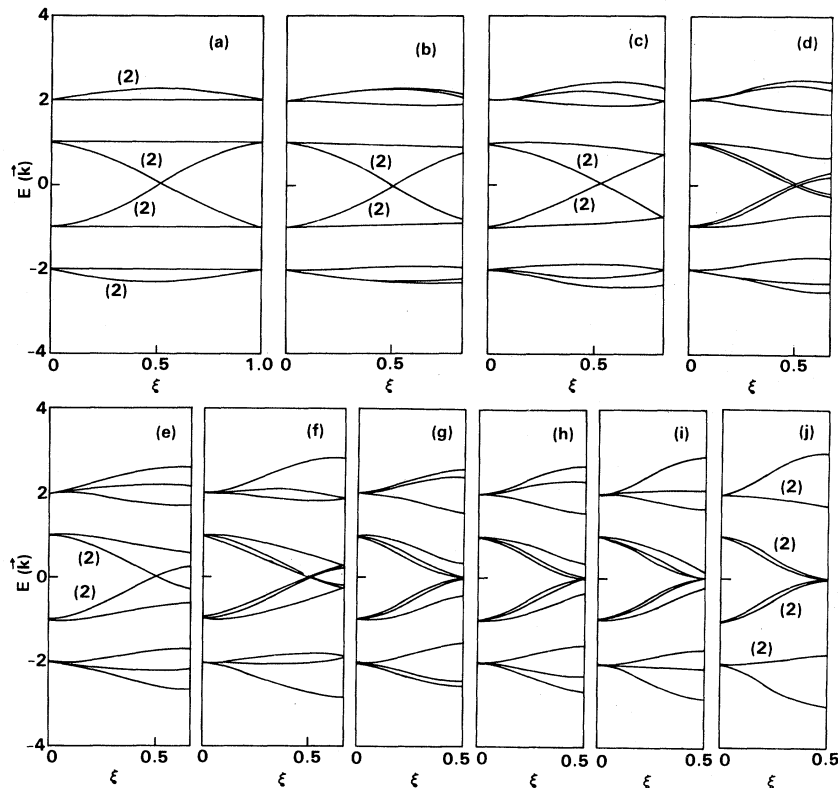


FIG. 5. Band structure $E(\vec{k})$ for the ω_{II} bands in nearest-neighbor approximation. Various slices of the Brillouin zone for \vec{k} along (a) [100], (b) $[1\frac{1}{5}0]$, (c) $[1\frac{1}{5}\frac{1}{5}]$, (d) $[1\frac{1}{2}0]$, (e) $[1\frac{1}{2}\frac{1}{5}]$, (f) $[1\frac{1}{2}\frac{1}{2}]$, (g) [110], (h) $[11\frac{1}{5}]$, (i) $[11\frac{1}{2}]$, (j) [111]. The energy scale is equal to the overlap integral H_{II} . As shown, the second parameter, $S=0.5$. (See text.) The zero of energy is equal to that of the isolated local oscillator, excited by an amount ω_{II} . $\vec{k}=(2\pi/a)(\xi, \eta, \zeta)$.

the effects of including second-nearest-neighbor integrals in the ω_{II} bands are illustrated in Fig. 6 for the case $T=U=0.2$. It is clear that the existence of pairs of eigenvalues at $\pm E$ is already removed by the inclusion of these small corrections. Also, the band crossings are lifted. However, vestiges of the pseudo-zone-boundary remain in the form of (some) zero slopes near (but not always precisely at) $\xi = \frac{1}{2}$.

When comparing the ω_I bands (Fig. 4) with the ω_{II} bands (Fig. 5 or Fig. 6), it is worth recalling that the zero of energy in the latter diagrams lies above that of the former by an amount $\omega_{II} - \omega_I = 0.4\omega_I$ and, also, that different scale factors, H_I and H_{II} , are employed as the units of energy for the ω_I and ω_{II} bands. From either Fig. 5 or Fig. 6, I obtain the

crude estimate $\Delta E_{II} = 6H_{II}$ for the width of the ω_{II} band, to be compared with the result $\Delta E_I = 8H_I$ for the ω_I band, whence

$$H_{II}/H_I = 1.3(\Delta E_{II}/\Delta E_I). \quad (36)$$

This relation is useful when comparing the results of the present theory with experiment in Sec. IV.

IV. COMPARISON WITH EXPERIMENT

The theory developed here is essentially a low-temperature theory, in the sense that thermally activated processes have been wholly neglected in the application to inelastic neutron scattering (cf. Sec. II). Since, for the systems considered in Refs. 3 and

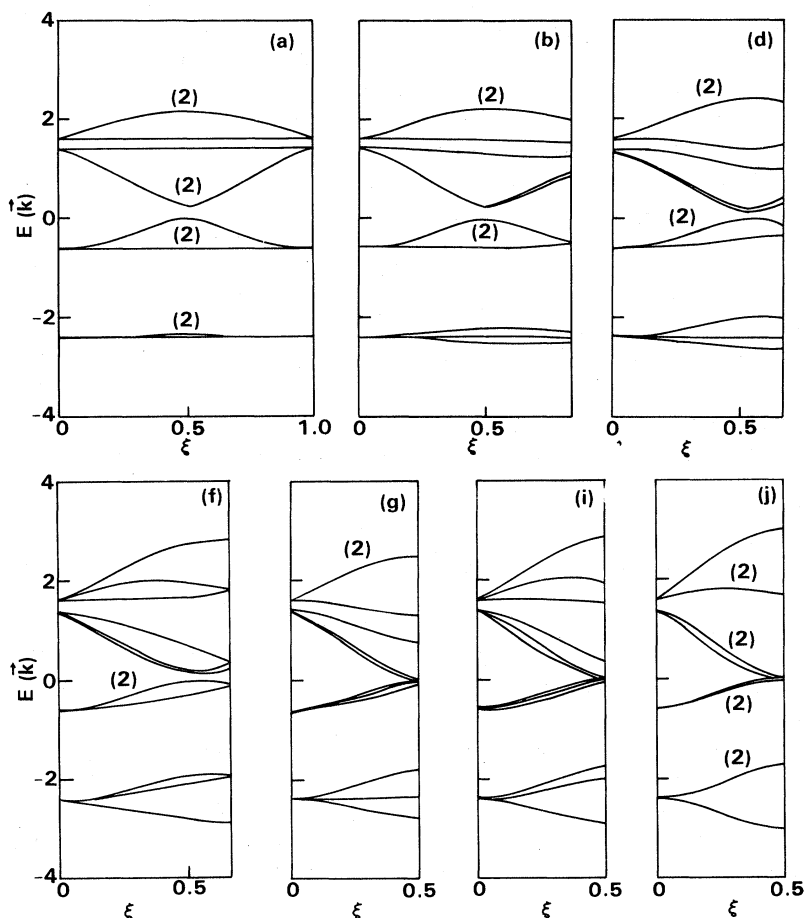


FIG. 6. Effect of second-nearest neighbor corrections on the band structure $E(\vec{k})$ for the ω_{II} bands. Subset of graphs for \vec{k} along (a) [100], (b) $[1\frac{1}{2}0]$, (d) $[1\frac{1}{2}0]$, (f) $[1\frac{1}{2}\frac{1}{2}]$, (g) [110], (i) $[11\frac{1}{2}]$, (j) [111]. Graphs are labeled to correspond with their designation in Fig. 5. $S=0.5$, $T=0.2$, $U=0.2$. (See text.) Energy scale and zero, as in Fig. 5. $\vec{k} = (2\pi/a)(\xi, \eta, \zeta)$.

4, $\omega_I = O(100 \text{ meV})$, the assumption that only the ground state is occupied is quite good, even at room temperature. However, much above 150 K, thermally activated processes play a role in broadening the final states, as is evidenced experimentally by the increased widths of the neutron energy-loss bands as the temperature is increased from 150 to 295 K. This increase in bandwidths has been observed for dilute hydrogen in niobium with intentionally added trapping centers (O, N, or V) which inhibit precipitation into the ϵ phase of NbH.³ Unfortunately, the ϵ phase transition prevents observation of neutron-induced transitions via scattering from hydrogen in the dilute α phase much below room temperatures. Thus direct comparison of the theory with low-temperature experiments on these dilutely hydrogenated, but otherwise nominally pure, bcc metals is not possible. Instead, the low-temperature data of the defected samples will be employed. Nevertheless, some qualitative statements can be made based upon the room temperature data for the pure samples. The lower lying ω_I band, although broadened by thermal processes, is less affected than the ω_{II} band. Hence, we may see whether the relative widths of the ω_I band, as observed by neutron scattering from dilute hydrogen in the nominally pure metals V, Nb, and Ta at room temperature, vary as we might expect by extrapolation of the theoretical predictions, which apply at low temperatures. Qualitatively, the answer appears to be in the affirmative. The lattice constant of V (3.03 Å) is $O(10\%)$ smaller than those of Nb (3.29 Å) and Ta (3.30 Å), which are nearly equal. Moreover, the excitation energies for all three systems are nearly the same, $O(100 \text{ meV})$, indicating that the local-oscillator potentials (as obtained by expansion of the full hydrogen-metal-lattice interaction potentials in the neighborhood of the vertices of the WS cell) are also nearly the same. Hence, the local-oscillator hydrogen wave functions have roughly the same extent and the overlap of these (Gaussian-damped) wave functions will be greater in V with its smaller lattice constant than for Nb or Ta, leading to a greater width for the excited-oscillator energy bands for V than for the other two. This prediction is obeyed experimentally.⁴ Among Nb and Ta, ω_I is $O(10\%)$ greater for Ta than for Nb, implying that its local-oscillator wave functions are somewhat more contracted in space. Neglecting the $O(0.3\%)$ difference in their lattice constants, the excited-oscillator hydrogen wave functions ought therefore to overlap less in Ta than in Nb, leading to narrower excited bands for Ta than for Nb, again in agreement with the neutron experiments.⁴

This qualitative agreement must be regarded with caution, however, since the theoretical bandwidths

depend upon overlap integrals, such as H_I , which contain the Hamiltonian operator [Eq. (2)] sandwiched between the off-center wave functions. Moreover, as discussed in the Introduction, the value of H_I for each metal depends upon the crystal potential in the regions of maximum overlap, where the strength of this potential need not be equal to the strength of the local oscillator potential near the vertices of the WS cell, whereas the latter determines ω_I . Nonetheless, the successful ordering in size of the ω_I bandwidths is encouraging.

What can be learned from the defected samples? Here, as a consequence of trapping, precipitation in ϵ -phase NbH is inhibited; hence, thermal effects can be minimized by going to lower temperatures. Also, by comparing the ratio Γ_{II}/Γ_I of the experimental widths in the *same* sample with the corresponding ratio $\Delta E_{II}/\Delta E_I$ of the theoretical bandwidths, semi-quantitative statements can be made. Of the systems studied in Ref. 3, the samples doped with V show evidence of precipitation to ϵ -NbH at $T=78$ K. Therefore, attention will be focused on the ratios $\Gamma_{II}/\Gamma_I=2.0$ for $\text{NbN}_{0.004}\text{H}_{0.003}$ at $T=10$ K and $\Gamma_{II}/\Gamma_I=1.3$ for $\text{NbO}_{0.011}\text{H}_{0.010}$ at $T=4$ K. I shall investigate the consequences of assuming that, at these temperatures, the major source of the experimental widths lies in the energy bandwidths I obtain and of neglecting the changes in these widths produced by the defects.⁸ Setting $\Delta E_{II}/\Delta E_I = \langle \Gamma_{II}/\Gamma_I \rangle = 1.7$ and employing Eq. (36). I find that, on the average, the value of the overlap integral H_{II} [Fig. 3(b) of Fig. 3] is roughly twice that of H_I [Fig. 3(a)]. This result is not unreasonable, as can be seen by superimposing either graph on the cube face with shaded interior in Fig. 1 and noting that the region of maximal wave-function overlap Fig. 3(b) lies quite close to the metal atom at the cube corner (labeled *a* in Fig. 1). In contrast, the center of the region of maximal wave-function overlap for Fig. 3(a) lies within the shaded area in Fig. 1, relatively farther away from its closest metal atoms (at *c* and *d* in Fig. 1).

Let Λ_I and Λ_{II} be the *wave-function* overlap integrals which result when the Hamiltonian operator given by Eq. (2) is replaced by the identity operator in the expressions for the overlap integrals H_I and H_{II} , respectively. Factoring each as illustrated by Eq. (4) and taking their ratio,

$$(H_{II}/H_I) = (\epsilon_{II}/\epsilon_I)(\Lambda_{II}/\Lambda_I). \quad (37)$$

By direct evaluation, it can be shown that

$$(\Lambda_{II}/\Lambda_I) = (\omega_I/\omega_{II}) = (\frac{1}{2})^{1/2}, \quad (38)$$

independently of the value of the lattice constant. Thus the ratio $(\epsilon_{II}/\epsilon_I)$ is roughly twice the ratio

(ω_{II}/ω_I) , showing that, in first approximation, not only are the scale factors ϵ_I and ϵ_{II} not equal to ω_I and ω_{II} , respectively (as was discussed in Sec. I), but also they fail to scale, albeit by only a factor of 2, in their *ratio*. Since the ratios of the experimental widths differ by nearly that much among samples with different defects, the discrepancy is not serious, but it is nonetheless interesting to see how higher order corrections might go. Not surprisingly, it turns out that the ratio Λ_{II}/Λ_I of the integrals is equal to the ratio of the corresponding integrands, taken with each integrand maximal. As mentioned in Sec. I, it seems reasonable that at these points the (repulsive) potential in the Hamiltonian [Eq. (2)] can be sufficiently large that, in *higher order*, the local wave functions approach zero in these regions and the overlap integrals H_I and H_{II} are dominated instead by contributions from the saddle-point regions of the potential, midway between the vertices of the WS cell. It so happens that, at these midpoints, the ratio of the products of the excited oscillator wave functions, i.e., the ratio of the integrands in Λ_{II} and Λ_I , equals ω_{II}/ω_I , the inverse of the corresponding ratio at their maximal values. It seems reasonable to assume that the integrands associated with the modified integrals Λ'_{II} and Λ'_I maintain this ratio at the midpoints, now dominating the integrals, which themselves exhibit this same ratio, i.e., that

$$\Lambda'_{II}/\Lambda'_I = \omega_{II}/\omega_I = 2^{1/2}. \quad (39)$$

Substitution of this modified ratio in Eq. (37), recalling that, given Eq. (36), (H_{II}/H_I) remains fixed (approximately equal to 2) by experiment, leads to a modified ratio of the scale factors, $\epsilon'_{II}/\epsilon'_I \simeq 2^{1/2}$. That is, in higher order the *ratio* ($\epsilon'_{II}/\epsilon'_I$) is expected to scale roughly as (ω_{II}/ω_I) , even though $\epsilon'_i \neq \omega_i$, $i=I,II$, for the reason cited in Sec. I and, again, earlier in the present discussion.

Turning the argument around, if I *assume* that in higher order the scale factors ϵ'_I and ϵ'_{II} in Eq. (4) are proportional to ω_I and ω_{II} , i.e.,

$$\epsilon'_{II}/\epsilon'_I = \omega_{II}/\omega_I, \quad (40)$$

and estimate the ratio of the corrected overlap integrals as given by Eq. (39), then from Eq. (37) I am led to *predict*

$$H_{II}/H_I = (\omega_{II}/\omega_I)^2 \simeq 2. \quad (41)$$

This relation, together with Eq. (36) leads to a *predicted ratio* $\Gamma_{II}/\Gamma_I = 1.5$ for the experimental widths, to be compared with $\langle \Gamma_{II}/\Gamma_I \rangle = 1.7$, as obtained from the data in Ref. 3. However, a fully quantitative discussion requires a folding in of the density of states for each band, rather than employing the crude estimates $\Delta E_I = 8H_I$, $\Delta E_{II} = 6H_{II}$,

which led to the factor 1.3 in Eq. (36). Also, some understanding of the variation of the widths as affected by the presence of the different defects (V, O, N in Nb) is required, neither of which is considered further here.

V. CONCLUSIONS

The hypothesis that the excited oscillator states of dilute hydrogen in bcc metals merge into bands appears compatible with experiment. In particular, I find the following: (i) When the hydrogen occupancy sites from a Bravais lattice, the differential cross section $d^2\sigma/d\Omega d\epsilon$ for inelastic neutron scattering associated with transitions to the excited-oscillator band states is equal to that for a single isolated oscillator when one substitutes the finite-width density of states function $g(E)$ for the Dirac δ function in the expression for the latter. In first approximation, this result also holds for the general case of several sites in the unit cell. (ii) The relation $\Gamma(V) > \Gamma(Nb) > \Gamma(Ta)$ among the experimental bandwidths for inelastic neutron scattering from these dilutely hydrogenated bcc metals is successfully predicted by the theory. (iii) The theoretical widths ΔE_I and ΔE_{II} of the excitation bands associated with the ω_I (nondegenerate) and ω_{II} (doubly degenerate) oscillator excitations depend mainly on only two irreducible overlap integrals, H_I and H_{II} . That is, $\Delta E_{II}/\Delta E_I = (H_{II}/H_I)\Upsilon$, where Υ is almost a universal constant of the bcc metals, depending only on the geometry of the tetrahedral hydrogen site occupancy in these metals. By inspection of the band structures given in Figs. 4–6, I estimate $\Upsilon \simeq \frac{3}{4}$. (iv) Based upon plausible, but less firmly based, assumptions concerning the nature of higher-order corrections, I am led to propose the relation $H_{II}/H_I = (\omega_{II}/\omega_I)^2$ [Eq. (41)] whence, given the model-consistent experimental relation $\omega_{II}/\omega_I = 2^{1/2}$, I predict $\Delta E_{II}/\Delta E_I \simeq \frac{3}{2}$. This prediction is in reasonable agreement with the experimental results, $\Gamma_{II}/\Gamma_I = 1.3$ and 2.0 for inelastic neutron scattering from dilute H in Nb associated with O and N impurities, respectively. Deviations are attributed to the effects of the different impurities on the intrinsic band structure.

ACKNOWLEDGMENTS

I have benefited from fruitful discussions with many of my colleagues in the Reactor Radiation Division of whom I wish particularly to thank J. Michael Rowe, John Rush, and Samuel Trevino. I also wish to thank Arnold Kahn for helpful comments.

- ¹This topic has been reviewed by H. Wipf and K. Neumaier, and by K. Kehr, in the Proceedings of the International Symposium on the Electronic Structure and Properties of Hydrogen in Metals, Richmond, Virginia, 1982 (unpublished). For general reviews, see *Hydrogen in Metals I and II*, Vols. 28 and 29 of *Topics in Applied Physics*, edited by G. Alefeld and J. Volkl (Springer, New York, 1978).
- ²H. Wipf, A. Magerl, S. M. Shapiro, S. K. Satija, and W. Thomlinson, *Phys. Rev. Lett.* **46**, 947 (1981).
- ³A. Magerl, J. J. Rush, J. M. Rowe, D. Richter, and H. Wipf, *Phys. Rev. B* **27**, 927 (1983). Peaks widths quoted therein are not corrected for instrumental resolution and have estimated errors of 1–2 meV (private communication).
- ⁴J. J. Rush, A. Magerl, and J. M. Rowe, *Bull. Am. Phys. Soc.* **26**, 337 (1981).
- ⁵R. C. Casella, *Phys. Rev. B* **24**, 2913 (1981). The effective scattering length \bar{a} is defined in Ref. 11 of this paper, where the symbol a is used.
- ⁶R. C. Casella, *J. Phys. (Paris) Colloq.* **42**, C6-923 (1981).
- ⁷There exists an experimental complication, however, in that at low temperatures measurements of dilute H in the α phase cannot be made, due to precipitation to the ϵ -NbH phase. This point is discussed further in Sec. IV. I thank J. J. Rush and J. M. Rowe for discussions on this point.
- ⁸Actually, a weaker assumption will do. It suffices to assume that whatever changes are induced in the widths ΔE_I and ΔE_{II} by the impurities, for each species, these changes tend to cancel in taking the ratio $\Delta E_{II}/\Delta E_I$. The value of the corresponding experimental ratio Γ_{II}/Γ_I changes with species by $O(50\%)$ (see Ref. 3). Therefore, I can only predict the average ratio $\langle \Gamma_{II}/\Gamma_I \rangle$ for the band widths, where the average is taken over samples with different trapping impurities.